Improved Hole Interfacial Layer for Planar Perovskite Solar Cells with Efficiency Exceeding 15%

ARTICLE *in* ACS APPLIED MATERIALS & INTERFACES · APRIL 2015

Impact Factor: 6.72 · DOI: 10.1021/acsami.5b01330 · Source: PubMed

6 AUTHORS, INCLUDING:

Zhao-Kui Wang
Soochow University (PRC)
90 PUBLICATIONS **456** CITATIONS
SEE PROFILE

Meng Li
Soochow University (PRC)
2 PUBLICATIONS **8** CITATIONS
SEE PROFILE

L. S. Liao
Soochow University, Suzhou, China
188 PUBLICATIONS **3,083** CITATIONS
SEE PROFILE

Heng Ma
Henan Normal University
41 PUBLICATIONS **109** CITATIONS
SEE PROFILE

ACS APPLIED MATERIALS & INTERFACES

Research Article

www.acsami.org

Improved Hole Interfacial Layer for Planar Perovskite Solar Cells with Efficiency Exceeding 15%

Zhao-Kui Wang,[†] Meng Li,[‡] Da-Xing Yuan,[†] Xiao-Bo Shi,[†] Heng Ma,[‡] and Liang-Sheng Liao*,[†]

[†]Jiangsu Key Laboratory for Carbon-Based Functional Materials & Devices, Institute of Functional Nano & Soft Materials (FUNSOM), Soochow University, Suzhou, Jiangsu 215123, China

[‡]College of Physics and Electronic Engineering, Henan Normal University, Xinxiang 453007, China

Supporting Information

ABSTRACT: Planar structure has been proven to be efficient and convenient in fabricating low-temperature and solution-processing perovskite solar cells (PSCs). Interface control and crystal film growth of organometal halide films are regarded as the most important factors to obtain high-performance PSCs. Herein, we report a solution-processed PEDOT:PSS-GeO_2 composite films by simply incorporating the GeO_2 aqueous solution into the PEDOT:PSS aqueous dispersion as a hole transport layer in planar PSCs. Besides the merits of high conductivity, ambient stability and interface modification of PEDOT:PSS-GeO_2 composite films, the formed island-like GeO_2 particles are assumed to act as growing sites of crystal nucleus of perovskite films during annealing. By the seed-mediation of GeO_2 particles, a superior $CH_3NH_3PbI_{3-x}Cl_x$ crystalline film with large-scale domains and good film uniformity was obtained. The resulting PSC device with PEDOT:PSS-GeO_2 composite film as HTL shows a best performance with 15.15% PCE and a fill factor (FF) of 74%. There is a remarkable improvement (~37%) in PCE, from 9.87% to 13.54% (in average for over 120 devices), compared with the reference pristine PEDOT:PSS based device.

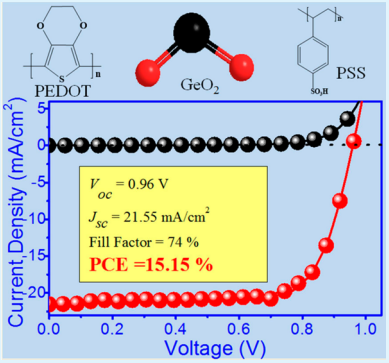

KEYWORDS: *perovskite solar cells, hole interfacial layer, solution-processing, GeO_2 nanoparticles*

1. INTRODUCTION

The studies of perovskite solar cells (PSCs) have recently made remarkable progress[1−4] because of their excellent optical and electronic properties of the perovskite materials, such as strong absorption in visible region[5,6] and long charge carrier diffusion length.[7−10] The power conversion efficiency (PCE) is increased dramatically from less than 4% to ~20.1% (certified) in the past five years.[11−19] In the initial work done by Kojima et al., alkylammonium metal trihalide perovskite absorbers was used in liquid electrolyte sensitized solar cells with a PCE of 3.8%.[11] Subsequently, solid-state configuration and TiO_2 and Al_2O_3 scaffolds based devices were proposed and employed successfully with over 10% in PCE.[20,21] Furthermore, a small molecule of 2,2′,7,7′-tetrakis(*N*,*N*-di-*p*-methoxyphenylamine)-9,9′-spirobifluorene (spiro-OMeTAD) was used as a hole transport layer by several groups with rapidly improved PCE over 15%.[22−27]

Most recently, perovskite solar cells based on planar structure also demonstrated remarkable efficiency over 10% by carrying out controllable interface engineering.[28−34] It was found that the planar structure can also facilitate a simple fabrication for low-temperature and solution-processing PSCs. It means that these planar structured PSCs can be made with reduced processing complexity of mesoporous TiO_2 or Al_2O_3 scaffolds in the previous PSC structures.[20,23] To date, most studies are focused on the perovskite film processing and relevant material design. As a matter of fact, the perovskite light-absorbing layer is sandwiched between the hole- and electron-transporting layers in a typical planar PSC.[33] Thus, for pursuing high PCE cells, it is essential to manipulate the carrier behaviors in whole perovskite solar cell. Therefore, the interface control plays very important role for device optimization in planar PSCs.

Poly(3,4-ethylenedioxy-thiophene)-poly(styrenesulfonate) (PEDOT:PSS) is a commonly used hole transport layer (HTL) for indium tin oxide (ITO) modification in conventional organic solar cells owing to its good conductivity and solution processability. However, the device stability is seriously restricted by the acidic (pH ≈ 2) nature of PEDOT: PSS dispersions.[35−37] Metal oxides materials have been reported to be the potential alternatives to replace PEDOT:PSS in organic electronics with the goal of improving device stability.[38,39] GeO_2 is also an excellent semiconductor material with good optical and electrical properties. However, the trial application of thermal evaporated GeO_2 in organic light-emitting diodes[40] and organic solar cells[41] as an interfacial layer demonstrated unsatisfactory effects because of its poor vacuum film-processing ability. Instead, we reported a solution-processed GeO_2 interfacial film, which exhibited superior device performance and stability in organic solar cells,[42] by adopting its slight solubility in water. PEDOT:PSS has its merits of high

Received: February 12, 2015
Accepted: April 21, 2015
Published: April 21, 2015

DOI: 10.1021/acsami.5b01330
ACS Appl. Mater. Interfaces 2015, 7, 9645−9651

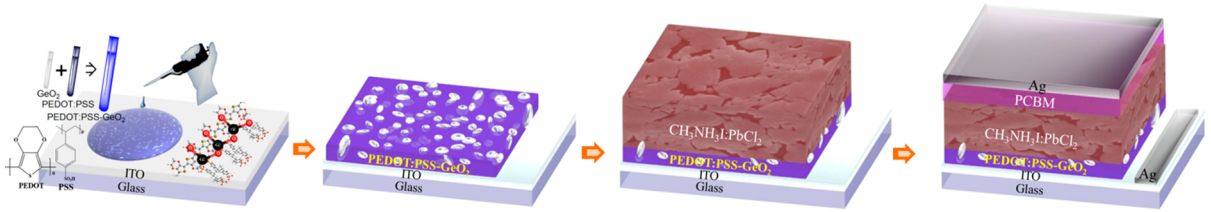

Figure 1. Flowchart of fabrication process for perovskite solar cells.

transparency, high work function, and high conductivity. GeO_2 has its own virture of near-alkaline pH value in its aqueous solution owing to a weak hydrolysis reaction as $GeO_2 + 2H_2O = Ge(OH)_4$. Therefore, a perfect (efficient and stable) hole interfaical film for perovskite solar cells is expected by mixing PEDOT:PSS and GeO_2 in aqueous solutions.

In this work, we report a solution-processed neutral PEDOT:PSS-GeO_2 composite films by simply incorporating GeO_2 aqueous solution into the PEDOT:PSS aqueous dispersion as an HTL in the planar perovskite solar cells. The PEDOT:PSS-GeO_2 composite films combine the advantage of high conductivity of PEDOT:PSS and the merit of ambient stability of GeO_2. In addition, the doped composite films can facilicate the carrier transport pathway from active layer to electrode from the viewpoint of interface contact. Herein, the aqueous solution-processed PEDOT:PSS-GeO_2 composite films are used as an anode interfacial layer in $CH_3NH_3PbI_{3-x}Cl_x$: phenyl-C61-butyric acid methyl ester (PCBM) based planar perovskite solar cells. The resulting PSC device with PEDOT:PSS-GeO_2 composite film as the HTL shows a best performance with 15.15% PCE and a fill factor (FF) of 74%. There is a remarkable improvement (~37%) in PCE, from 9.87% to 13.54% (in average for over 120 devices), compared with the reference pristine PEDOT:PSS based device. In addition, the cell with PEDOT:PSS-GeO_2 HTL demonstrates obviously improved stability compared with the reference device.

2. EXPERIMENTAL SECTION

2.1. Materials and Preparation. GeO_2 power was purchased from Shanghai Chemical Industry Co. Clevios PVP AL 4083 PEDOT:PSS was bought from Heraeus (Germany). $PbCl_2$ (99.999%), *N*,*N*-dimethylformamide (DMF) (anhydrous, amine free; 99.9%) were purchased from Alfa-Aesar. $PC_{61}BM$ was produced by Nichem Fine Technology Co., Ltd. (Taiwan). $PC_{61}BM$ was produced by Nichem Fine Technology Co., Ltd. (Taiwan). GeO_2 aqueous solutions were first prepared by dissolving GeO_2 powder directly into deionized water with over 10 h stirring in air at room temperature with an optimized concentration of 0.3 wt %. The prepared GeO_2 aqueous solutions were then blended into the PEDOT:PSS solution with different various volume ratios. A mixture of hydroiodic acid (57 wt % in H_2O) and methylamine (40% in methanol) was stirred in the ice bath for 2 h and evaporated at 70 °C for 1 h. The resulting product was washed for 1 h with diethyl ether and filtered. To improve purity, we dissolved the product in methanol (~100 mL), and the methanol solution containing CH_3NH_3I was dropped into diethyl ether (~1000 mL).[10] Then, CH_3NH_3I and $PbCl_2$ were dissolved in DMF with a molar ratio of 3:1. The mixture was stirred at 60 °C overnight in a glovebox.

2.2. Device and Characteristics. Solar cell devices were fabricated on patterned ITO-coated glass substrates with a sheet resistance of ~15 Ω/sq ITO were cleaned with a neutral detergent, followed by a sonication in a bath containing ethanol and then treated in UV-Ozone cleaner for 15 min. PEDOT:PSS-GeO_2 composite films were obtained by spin-coating the precursor on ITO surface under 4500 rpm/40 s and then annealing at 120 °C for 10 min. For the perovskite layer, 30 wt % $CH_3NH_3PbI_{3-x}Cl_x$ was spin coated from a dimethylformamide (DMF) solution with CH_3NH_3I (synthesized in a previous study) and $PbCl_2$ in a 3:1 molar ratio. The solution was spin-coated onto the hole transport layer at 4000 rpm for 40 s in a N_2 glovebox. The annealing of wet perovskite films was carried out by following a typcial gradient increased temperature method that can be seen elsewhere.[43] After it was dried at room temperature for ~20 min, the samples were slowly heated from 50 to 100 °C at a ramp rate of 10 °C/10 min on a hot plate. After that, 20 mg/mL PCBM in chlorobenzene solution was coated onto the perovskite layer at 2000 rpm for 40s in a N_2 glovebox. Finally, the samples were transferred to a vacuum chamber for Silver electrode evaporation. Ag (100 nm) was thermally deposited onto the PCBM layer under vacuum at 2×10^{-6} Torr through a shadow mask, defining a device area of 7.25 mm^2.

AFM images using a Veeco Multimode V instrument were obtained to evaluate the surface morphology of PEDOT:PSS-GeO_2 films. UPS analysis was carried out for evaluating the work function with an unfiltered He I (21.2 eV) gas discharge lamp and a hemispherical analyzer. The transmittance and absorption spectra of PEDOT:PSS:-GeO_2 and $CH_3NH_3PbI_{3-x}Cl_x$ films were measured with an UV/vis spectrophotometer (PerkinElmer Lambda 750). The surface morphologies of PEDOT:PSS:GeO_2 and $CH_3NH_3PbI_{3-x}Cl_x$ films was characterized by field-emission scanning electron microscopy (FE-SEM, Quanta 200 FEG, FEI Co.). Current density−voltage characteristics of PSCs under 1 sun illumination were performed in ambient condition using a programmable Keithley 2400 source meter under AM 1.5G solar irradiation at 100 mW/cm^2 (Newport, Class AAA solar simulator, 94023A-U). The stabilities of OSCs devices without encapsulation were evaluated in different conditions.

3. RESULTS AND DISCUSSION

3.1. PEDOT:PSS-GeO_2 Composite Films Film. Figure 1 shows a flowchart of fabrication process for perovskite solar cells including the preparation of PEDOT:PSS-GeO_2 composite films. GeO_2 aqueous solutions were prepared following a facile procedure by dissolving GeO_2 powder directly into deionized water with over 10 h stirring in air at room temperature with an optimization concentration of 0.3 wt % (Supporting Information Figure S1 and Table S1). The obtained GeO_2 aqueous solution was added simply into commercial PEDOT:PSS water dispersion (Clevios PVP AL 4083) with different mixing ratio. The PEDOT:PSS-GeO_2 composite films were then deposited by spin-coating the mixed solution onto cleared ITO with thermal annealing at 120 °C for 10 min in air.

Figure 2a and b shows the atomic force microscopy (AFM) surface morphology (5 × 5 μm) of pristine PEDOT:PSS film and PEDOT:PSS-GeO_2 (4:1 in volume ratio) composite film, respectively. The surface roughness (in root-mean-square, RMS) of pristine PEDOT:PSS film is 1.7 nm, whereas 3.6 nm for PEDOT:PSS-GeO_2 (4:1) composite film. The increased RMS is attributed to the islands formation on the PEDOT:PSS-GeO_2 surface. Noticeably, when increasing the mixing ratio of GeO_2, the roughness of the PEDOT:PSS-GeO_2 composite films is increased, whereas the islands diameter is decreased.

DOI: 10.1021/acsami.5b01330
ACS Appl. Mater. Interfaces 2015, 7, 9645−9651

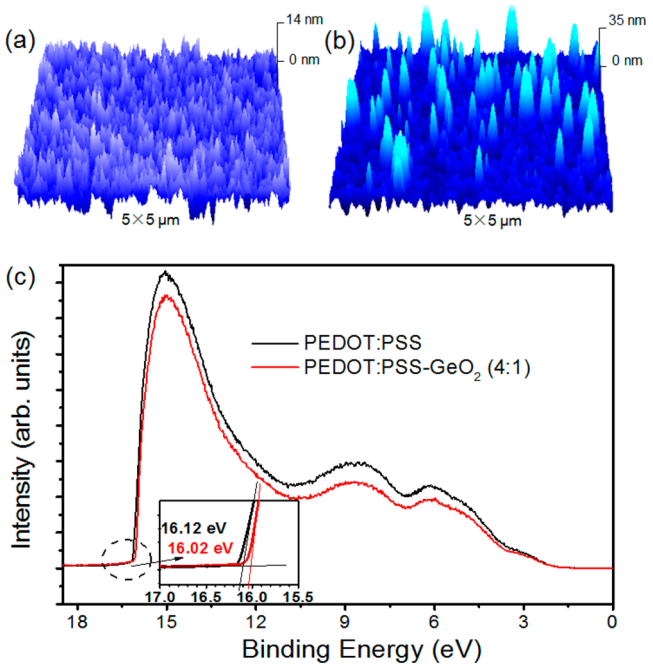

Figure 2. Atomic force microscopy (AFM) surface morphology (5 × 5 μm) of (a) pristine PEDOT:PSS film, (b) PEDOT:PSS-GeO_2 (4:1 in volume ratio) composite film, and (c) their corresponding UPS spectra. The inset is the enlarged secondary-electron cutoffs.

(Supporting Information Figure S2). The ultraviolet photoelectron spectroscopy (UPS) measurements of a pristine PEDOT:PSS film and the PEDOT:PSS-GeO_2 (4:1) composite film on ITO substrates were carried out and the results are shown in Figure 2c, where the inset is the magnified region of the photoemission cutoff. The work function of PEDOT:PSS-GeO_2 (4:1) composite films was determined to be 5.2 eV, which is slightly higher than that of the pristine PEDOT:PSS (5.1 eV). An increased work function at the anode interface side can result in a better energy alignment between ITO and perovskite active layer.

3.2. Perovskite Photovoltaic Performance. The mixed halide perovskite, $CH_3NH_3PbI_{3-x}Cl_x$, is used as a model system to investigate the effects of organic−inorganic (PEDOT:PSS-GeO_2) hybrid doping for highly efficient and stable perovskite solar cells. The devices have a strucutre of ITO/PEDOT:PSS (with or without GeO_2)/$CH_3NH_3PbI_{3-x}Cl_x$/PCBM/Ag (100 nm). The $CH_3NH_3PbI_{3-x}Cl_x$ solution ($CH_3NH_3I/PbCl_2$ = 3:1) was spin coated from a dimethylformamide (DMF) solution onto the PEDOT:PSS-GeO_2 composite films in a N_2 glovebox. Thermal annealing of the wet perovskite films was carried out by following a typical gradient increased temperature method that can be seen elsewhere.[43,44] Low-temperature (<100 °C) processed annealing is adopted to preserve the long charge carrier diffusion lengths of the perovskite absorbers.[45]

To investigate the GeO_2 doping effects, $CH_3NH_3PbI_{3-x}Cl_x$ solar cells based on PEDOT:PSS-GeO_2 hybrid HTLs with varied doping ratio were fabricated. The photovoltaic performance of $CH_3NH_3PbI_{3-x}Cl_x$ solar cells based on pristine PEDOT:PSS and PEDOT:PSS-GeO_2 hybrid HTLs with varied doping ratio is shown in Figure 3. The $J-V$ characteristics of all devices under AM 1.5G illumination with light intensity of 100 mW/cm^2 are shown in Figure 3a. The key cell parameters in these devices are listed in Table 1. The reference device using pristine PEDOT:PSS as an HTL showed a best PCE of 10.97% (short circuit current density of 18.57 mA/cm^2, open circuit voltage 0.89 V, and fill factor 0.67) and an average power conversion efficiency (PCE_{AVE}) (32 devices) of 9.87%. The performance of PEDOT:PSS-GeO_2 HTL based cells is

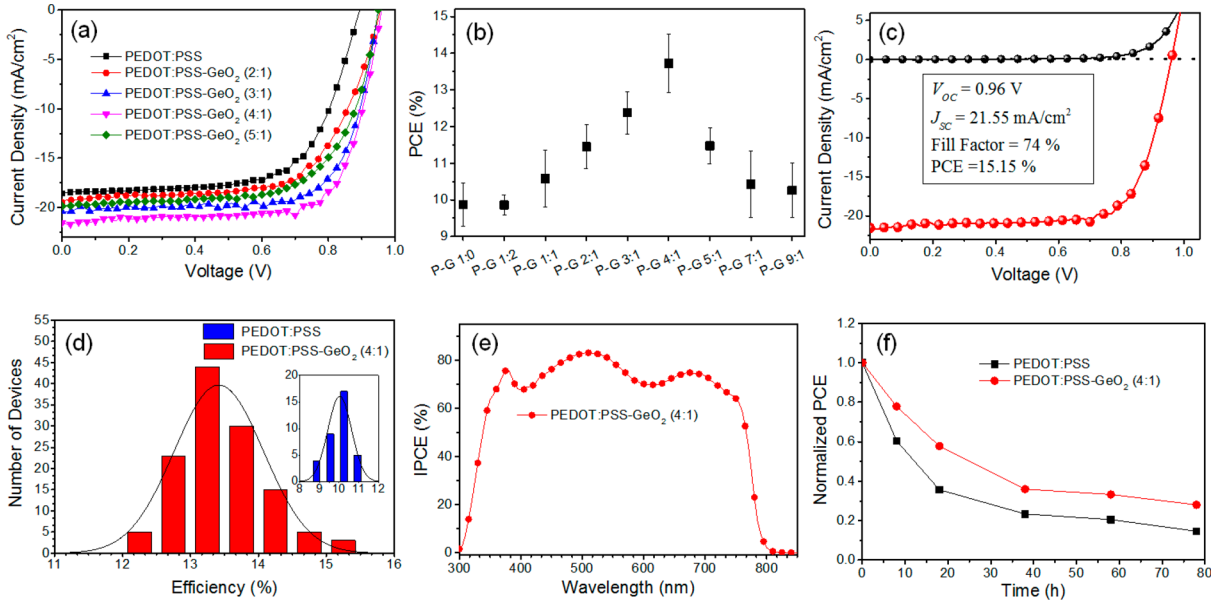

Figure 3. Performance and reproductivity of perovskite solar cells. (a) $J-V$ curves of devices with selected doping raito of GeO_2 in PEDOT:PSS as HTLs under AM 1.5G illumination of 100 mW/cm^2. (b) Plot of GeO_2 doping ratio depdendent power conversion efficiency (PCE). (c) $J-V$ curves of our champion device under AM 1.5G illumination of 100 mW/cm^2 (red line) and in the dark (black line). (d) A histogram of PCEs measured from 120 PEDOT:PSS-GeO_2 (4:1) HTL controlled devices. Inset is the histogram of PCEs measured from 32 PEDOT:PSS HTL based devices. (Gaussian distributions were fit to obtain the average and relative standard deviations.) (e) Incident photon-to-electron conversion efficiency (IPCE) curve of our champion device. (f) The normalized PCE values as a function of illuminating time in the devices using PEDOT:PSS and PEDOT:PSS-GeO_2 (4:1) as HTLs.

DOI: 10.1021/acsami.5b01330
ACS Appl. Mater. Interfaces 2015, 7, 9645−9651

Table 1. Photovoltaic Parameters of Perovskite Devices with Selected Doping Ratio of GeO_2 in PEDOT:PSS as HTLs

device	J_{SC} (mA/cm^2)	$J_{SC\text{-}AVE}$ (mA/cm^2)	V_{OC} (V)	FF	PCE (%)	PCE_{AVE} (%)	R_S (Ω)
PEDOT:PSS 40 nm	18.57	18.77 ± 0.62	0.89	0.67	10.97	9.87 ± 0.61	118.69
PEDOT:PSS-GeO_2 (5:1) 36 nm	19.84	19.94 ± 0.38	0.94	0.67	12.50	11.52 ± 0.56	62.98
PEDOT:PSS-GeO_2 (4:1) 32 nm	21.55	20.57 ± 0.42	0.96	0.74	15.15	13.54 ± 0.70	36.43
PEDOT:PSS-GeO_2 (3:1) 28 nm	20.39	19.84 ± 0.69	0.95	0.72	13.86	12.23 ± 0.49	67.86
PEDOT:PSS-GeO_2 (2:1) 25 nm	19.44	19.24 ± 0.42	0.96	0.65	12.10	11.45 ± 0.59	84.33

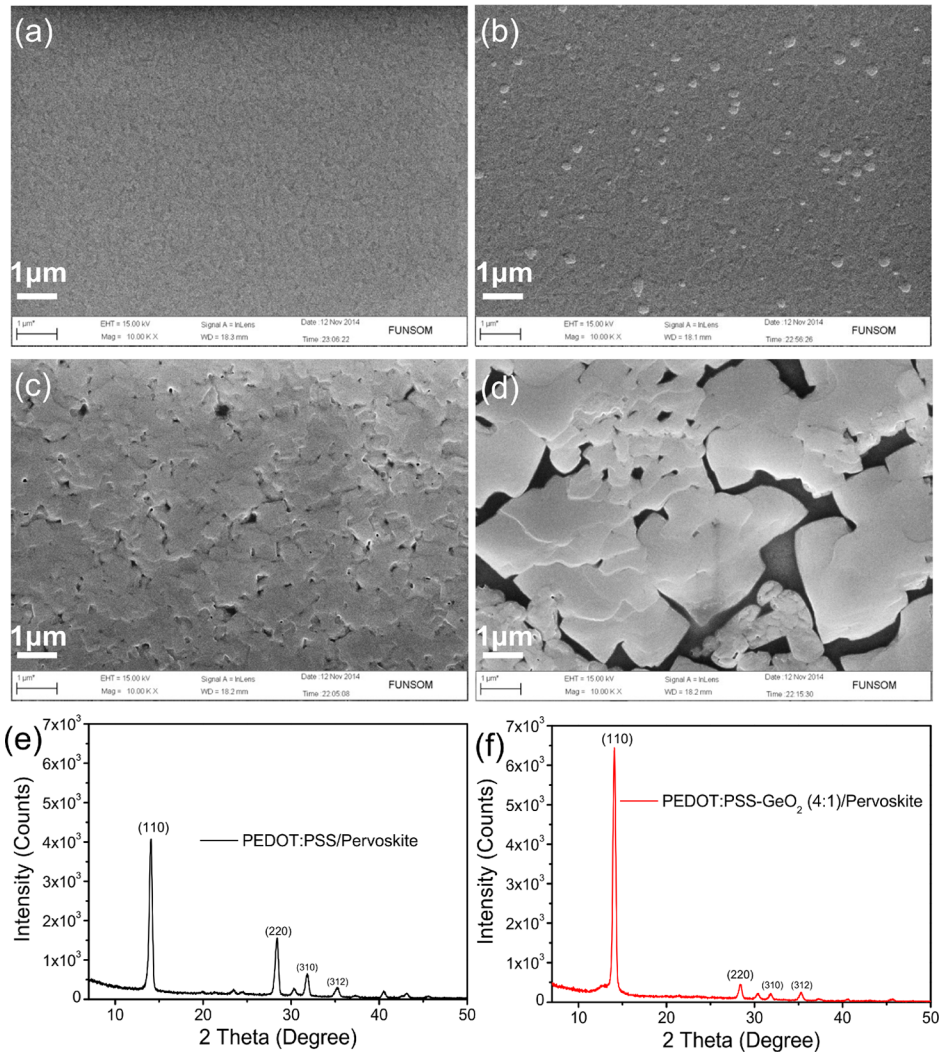

Figure 4. SEM images of (a) PEDOT:PSS film, (b) PEDOT:PSS-GeO_2 (4:1) film, (c) crystalline $CH_3NH_3PbI_{3-x}Cl_x$ film deposited on PEDOT:PSS, (d) crystalline $CH_3NH_3PbI_{3-x}Cl_x$ film deposited on PEDOT:PSS-GeO_2, and XRD patters of (e) crystalline $CH_3NH_3PbI_{3-x}Cl_x$ film deposited on PEDOT:PSS and (f) crystalline $CH_3NH_3PbI_{3-x}Cl_x$ film deposited on PEDOT:PSS-GeO_2.

dependent strongly on the doping ratio of GeO_2 in PEDOT:PSS, which can be clearly reflected in the PCE vs GeO_2 doping ratio plot as shown in Figure 3b and Supporting Information Table S2. The maximum performance was obtained at the doping ratio of 4:1 in volume for PEDOT:PSS-GeO_2, which resulted in a champion device exhibiting 15.15% power conversion efficiency, short circuit current density (J_{SC}) 21.55 mA/cm^2, open circuit voltage (V_{OC}) 0.96 V, and fill factor (FF) 0.74 under 100 mW/cm^2 AM 1.5 illumination (Figure 3c).

For verifying the reproducibility of high efficiency, over 120 $CH_3NH_3PbI_{3-x}Cl_x$ solar cells incorporating PEDOT:PSS-GeO_2 (4:1) HTLs were fabricated and tested. The average power conversion efficiency for this optimum doping ratio is 13.54% as shown in Table 1. All the devices were tested without any encapsulation under ambient conditions. As shown by the histograms of PCE parameter (Figure 3d) for reference devices (32 cells) and controllable devices (120 cells), the device performance followed a Gaussian distribution and yielded average PCE of 9.87% and 13.54% for the reference devices and the PEDOT:PSS-GeO_2 based devices, respectively. A remarkable 35% improvement in PCE_{AVE} (from 9.87% to 13.54%) is achieved. Relative standard deviations of 5.9% and 4.5% for the reference devices and the PEDOT:PSS-GeO_2 based devices, respectively, indicated that PEDOT:PSS-GeO_2 based devices showed much better reproducibility than that of the reference devices. The external quantum efficiency (EQE) spectrum of the champion device is shown in Figure 3e. Integrating the

DOI: 10.1021/acsami.5b01330
ACS Appl. Mater. Interfaces 2015, 7, 9645−9651

overlap of the EQE spectrum with the AM 1.5G solar photon flux generates a current density of 20.13 mA/cm^2, which is close to the measured short circuit photocurrent density of 21.55 mA/cm^2. In addition, the PCE for the reverse scan from the forward bias to short-circuit is higher than that of the forward scan from short-circuit to forward bias (Supporting Information Figure S3). This anomalous hysteresis is often observed in the current−voltage measurements of perovskite solar cells, and the origin is not clearly understood presently.[46]

In addition, as shown in Figure 3f, PEDOT:PSS-GeO_2 HTL based devices were found to be more stable than the pristine PEDOT:PSS based ones regardless under ambient air (dark), ambient air (light) and nitrogen conditions (Supporting Information Figure S4). The half-efficiency (half of initial efficiency of the fresh devices) of the reference device was reached rapidly just after 14 h of air exposure, whereas 26 h for the controlled device (Figure 3f). There was almost two times improvement in the cell stability by using PEDOT:PSS-GeO_2 (4:1) composite as the HTL in perovskite solar cells. A series of stability tests in different conditions were carried out (Supporting Information Figure S4). The statistical results demonstrated that PEDOT:PSS-GeO_2 based devices really improved the cell stability. Actually, the pH value of PEDOT:PSS-GeO_2 aqueous solution was dependent on the GeO_2 doping concentration (Supporting Information Table S5). For example, the pH value was increased from 1.92 (the case of pure PEDOT:PSS) to 3.56 when introducing GeO_2 into PEDOT:PSS (the case of PEDOT:PSS-GeO_2 (4:1)). The acidity was suppressed partly by the addition of GeO_2. However, the PEDOT:PSS-GeO_2 dispersion was still acidic in nature. Therefore, PEDOT:PSS-GeO_2 HTM based cells just demonstrated improved stability at some extent.

3.3. Mechanism of Improved Cell Performance. As aforementioned, the planar $CH_3NH_3PbI_{3-x}Cl_x$ solar cells incorporating PEDOT:PSS-GeO_2 (4:1) HTL exhibited substantial enhancement in power conversion efficiency and improvement in cell stability. From Table 1, we can see that the enhancement in PCE from 10.97% to 15.15% is associated with the increases of all three key parameters J_{SC} (18.57 to 21.55 mA/cm^2), V_{OC} (0.89 to 0.96 V), and FF (0.67 to 0.74), simultaneously. We assume that GeO_2 doped PEDOT:PSS HTL played a comprehensive role in interfacial contact and film crystallization of the perovskite layer for remarkable improvement in PCE. Herein, we carried out basis measurements and analysis of crystalline morphology evaluation of perovskite films, current−voltage characteristics, and time-resolved photoluminescence spectroscopy to clarify the role of GeO_2 doping into PEDOT:PSS HTL in improved performance of the planar $CH_3NH_3PbI_{3-x}Cl_x$ solar cells.

From AFM observation, there were island-like particles existed on PEDOT:PSS-GeO_2 composite films. The formation of islands can be clearly confirmed by scan electron microscopy (SEM). As shown in Figure 4b, the particles have the diameter varying in the range of 80−100 nm. We assume that these island-like particles were originated from the introducting of GeO_2 into PEDOT:PSS. Interestingly, we found that the crystallization of $CH_3NH_3PbI_{3-x}Cl_x$ films was affected strongly by their underlayer films. Figure 4c and 4d shows the SEM images of $CH_3NH_3PbI_{3-x}Cl_x$ films after annealing on the pristine PEDOT:PSS film and the PEDOT:PSS-GeO_2 composite film, respectively. The morphological differences between the $CH_3NH_3PbI_{3-x}Cl_x$ films on pristine PEDOT:PSS film and PEDOT:PSS-GeO_2 underlayers are very evident. $CH_3NH_3PbI_{3-x}Cl_x$ film on the pristine PEDOT:PSS film shows high coverage accompanying with many small pin-holes. The film is composed of interconnected nanoscale domains with sizes ranging from 0.7 to 1.2 μm. These defects can introduce strong energy disorder, which hinders the charge transport and induces carrier recombination, resulting in lower photovoltaic performance. In the $CH_3NH_3PbI_{3-x}Cl_x$ film on PEDOT:PSS-GeO_2 underlayer, however, we observed crystal $CH_3NH_3PbI_{3-x}Cl_x$ film with superior quality. Individual crystal size (3−5 μm) has been surprisingly increased, which is significatnly larger than the case of the reference one. Notably, laminar structure based perovskite crystal films with good grain boundary were observed. In addition, there exists wide boundary gaps (200−700 nm) among the large crystalline domains. The boundary gaps may not be helpful for the perovskite layer to absorb more light because of the existing voids without refiling with the righ materials. It is therefore expected that further enhancement might be achievable if the voids could be eliminated. We attributed the improved crystallization of $CH_3NH_3PbI_{3-x}Cl_x$ films to the introduciton of GeO_2 into PEDOT:PSS. As seen in Figure 2b and Figure 4b, the island-like GeO_2 particles distribute randomly on the surface of PEDOT:PSS-GeO_2 composite films. Seed-mediated growth method by adopting nanoparticles has been widely used in controlling the film growth for producing highly crystalline films.[46−48] We assume that these island-like GeO_2 particles could be acted as the growing sites of crystal nucleus of $CH_3NH_3PbI_{3-x}Cl_x$ films during annealing. By the seed-mediation of GeO_2 particles, a superior quality of $CH_3NH_3PbI_{3-x}Cl_x$ crystalline films with large-scale domains and good film unifromity was obtained as shown in Figure 4d. XRD results shown in Figure 4e and 4f confirm the improved crystallinity of the perovskite films. Unlike the pattern of $CH_3NH_3PbI_{3-x}Cl_x$ film deposited on the pristine PEDOT:PSS which displays many crystallographic planes including (110), (200), (211), (202), (220), (310), (312), (224), and (314), the one deposited on PEDOT:PSS-GeO_2 is dominated by the (110), (220), (310), and (312) peaks, especially by the (110) peak. It suggests that the $CH_3NH_3PbI_{3-x}Cl_x$ film deposited on PEDOT:PSS-GeO_2 grew preferentially along ⟨110⟩ with greater texture,[49] which is agreed well with the SEM observations. Good film crystalline means a better absorption for $CH_3NH_3PbI_{3-x}Cl_x$ film, which was cofirmed by the absorption spectra measurements (Supporting Information Figure S5).

4. CONCLUSION

We have demonstrated a solution-processed neutral PEDOT:PSS-GeO_2 composite films as an hole transport layer in the planar perovskite solar cells by simply incorporating the GeO_2 aqueous solution into the PEDOT:PSS aqueous dispersion. The resulting cells shows a best performance with 15.15% PCE and a fill factor (FF) of 74%. In average PCE (over 120 devices), there is a remarkable improvement (~37%) from 9.87% to 13.54% compared with the pristine PEDOT:PSS based device. From AFM and SEM evaluations, the formed island-like GeO_2 particles on PEDOT:PSS-GeO_2 surface are assumed to act as growing sites of crystal nucleus of perovskite films during thermal annealing. By the seed-mediation of GeO_2 particles, improved $CH_3NH_3PbI_{3-x}Cl_x$ crystalline films with large-scale domains and good film uniformity was obtained, which could explain the higher short-circuit current density, higher open-circuit voltage and higher fill factor of the

DOI: 10.1021/acsami.5b01330
ACS Appl. Mater. Interfaces 2015, 7, 9645−9651

corresponding solar cells. A study on the detailed role of GeO_2 seed-mediation in the growth of superior crystalline perovskite films is in progress.

■ ASSOCIATED CONTENT

Supporting Information

Performance of pristine GeO_2 based perovskite solar cells, AFM top images of PEDOT:PSS-GeO_2 films with varied GeO_2 doping ratio, doping ratio optimization of the PEDOT:PSS-GeO_2, reverse- and forward-scan based $J-V$ curves, device stabilities evaluated under different circumstance, absorption coefficients of the pristine and the controlled $CH_3NH_3PbI_{3-x}Cl_x$ films, thickness optimization of the PEDOT:PSS-GeO_2 interfacial layer are provided. The Supporting Information is available free of charge on the ACS Publications website at DOI: 10.1021/acsami.5b01330.

■ AUTHOR INFORMATION

Corresponding Author

*E-mail: lsliao@suda.edu.cn.

Author Contributions

Z.-K.W. and M.L. contributed equally to the work.

Notes

The authors declare no competing financial interest.

■ ACKNOWLEDGMENTS

We acknowledge financial support from the Natural Science Foundation of China (Nos. 61307036 and 61177016) and from the Natural Science Foundation of Jiangsu Province (No. BK20130288). This project is also funded by the Collaborative Innovation Center of Suzhou Nano Science and Technology, and by the Priority Academic Program Development of Jiangsu Higher Education Institutions (PAPD).

■ REFERENCES

(1) Kazim, S.; Nazeeruddin, M. K.; Grätzel, M.; Ahmad, S. Perovskite as Light Harvester: A Game Changer in Photovoltaics. *Angew. Chem. Int. Ed.* **2014**, *53*, 2812−2824.

(2) Snaith, H. J. Perovskites: The Emergence of a New Era for Low-Cost, High-Efficiency Solar Cells. *J. Phys. Chem. Lett.* **2013**, *4*, 3623−3630.

(3) Park, N.-G. Organometal Perovskite Light Absorbers Toward a 20% Efficiency Low-cost Solid-State Mesoscopic Solar Cell. *J. Phys. Chem. Lett.* **2013**, *4*, 2423−2429.

(4) Gao, P.; Grätzel, M.; Nazeeruddin, M. K. Organohalide Lead Perovskites for Photovoltaic Applications. *Energy Environ. Sci.* **2014**, *7*, 2448−2463.

(5) Mitzi, D. B. Synthesis, Structure, and Properties of Organic−Inorganic Perovskites and Related Materials. *Prog. Inorg. Chem.* **2007**, *48*, 1−121.

(6) Sum, T. C.; Mathews, N. Advancements in Perovskite Solar Cells: Photophysics Behind the Photovoltaics. *Energy Environ. Sci.* **2014**, *7*, 2518−2534.

(7) Stranks, S. D.; Eperon, G. E.; Giulia, G.; Christopher, M.; Alcocer, M. J.; Tomas, L.; Herz, L. M.; Annamaria, P.; Snaith, H. J. Electron−Hole Diffusion Lengths Exceeding 1 Micrometer in an Organometal Trihalide Perovskite Absorber. *Science* **2013**, *342*, 341−344.

(8) Xing, G.; Mathews, N.; Sun, S.; Lim, S. S.; Lam, Y. M.; Grätzel, M.; Mhaisalkar, S.; Sum, T. C. Long-Range Balanced Electron-and Hole-Transport Lengths in Organic-Inorganic $CH_3NH_3PbI_3$. *Science* **2013**, *342*, 344−347.

(9) Zhao, Y.; Zhu, K. Charge Transport and Recombination in Perovskite $(CH_3NH_3)PbI_3$ Sensitized TiO_2 Solar Cells. *J. Phys. Chem. Lett.* **2013**, *4*, 2880−2884.

(10) Wehrenfennig, C.; Eperon, G. E.; Johnston, M. B.; Snaith, H. J.; Herz, L. M. High Charge Carrier Mobilities and Lifetimes in Organolead Trihalide Perovskites. *Adv. Mater.* **2014**, *26*, 1584−1589.

(11) Kojima, A.; Teshima, K.; Shirai, Y.; Miyasaka, T. Organometal Halide Perovskites as Visible-Light Sensitizers for Photovoltaic Cells. *J. Am. Chem. Soc.* **2009**, *131*, 6050−6051.

(12) Burschka, J.; Pellet, N.; Moon, S.-J.; Humphry-Baker, R.; Gao, P.; Nazeeruddin, M. K.; Grätzel, M. Sequential Deposition as a Route to High-Performance Perovskite-Sensitized Solar Cells. *Nature* **2013**, *499*, 316−319.

(13) Liu, M.; Johnston, M. B.; Snaith, H. J. Efficient Planar Heterojunction Perovskite Solar Cells by Vapour Deposition. *Nature* **2013**, *501*, 395−398.

(14) Liu, D.; Kelly, T. L. Perovskite Solar Cells with a Planar Heterojunction Structure Prepared Using Room-Temperature Solution Processing Techniques. *Nat. Photonics* **2014**, *8*, 133−138.

(15) Wang, J. T.-W.; Ball, J. M.; Barea, E. M.; Abate, A.; Alexander-Webber, J. A.; Huang, J.; Saliba, M.; Mora-Sero, I.; Bisquert, J.; Snaith, H. J.; Nicholas, R. J. Low-Temperature Processed Electron Collection Layers of Graphene/TiO_2 Nanocomposites in Thin Film Perovskite Solar Cells. *Nano Lett.* **2013**, *14*, 724−730.

(16) Wojciechowski, K.; Saliba, M.; Leijtens, T.; Abate, A.; Snaith, H. J. Sub-150°C Processed Meso-Superstructured Perovskite Solar Cells with Enhanced Efficiency. *Energy Environ. Sci.* **2014**, *7*, 1142−1147.

(17) Nie, W.; Tsai, H.; Asadpour, R.; Blancon, J.; Neukirch, A. J.; Gupta, G.; Crochet, J. J.; Chhowalla, M.; Tretiak, S.; Alam, M. A.; Wang, H.; Mohite, A. D. High-Efficiency Solution-Processed Perovskite Solar Cells With Millimeter-Scale Grains. *Science* **2015**, *437*, 522−525.

(18) Jeon, N. J.; Noh, J. H.; Yang, W. S.; Kim, Y. C.; Ryu, S.; Seo, J.; Seok, S. I. Compositional Engineering of Perovskite Materials For High-Performance Solar Cells. *Nature* **2015**, *517*, 476−480.

(19) National Renewable Energy Laboratory, 2015. www.nrel.gov/ncpv/images/efficiency_chart.jpg.

(20) Etgar, L.; Gao, P.; Xue, Z. S.; Peng, Q.; Chandiran, A. K.; Liu, B.; Nazeeruddin, M. K.; Grätzel, M. Mesoscopic $CH_3NH_3PbI_3/TiO_2$ Heterojunction Solar Cells. *J. Am. Chem. Soc.* **2012**, *134*, 17396−17399.

(21) Kim, H. S.; Lee, C. R.; Im, J. H.; Lee, K. B.; Moehl, T.; Marchioro, A.; Moon, S. J.; Humphry-Baker, R.; Yum, J. H.; Moser, J. E.; Grätzel, M.; Park, N. G. Lead Iodide Perovskite Sensitized All-Solid-State Submicron Thin Film Mesoscopic Solar Cell with Efficiency Exceeding 9%. *Sci. Rep.* **2012**, *2*, 591.

(22) Lee, M. M.; Teuscher, J.; Miyasaka, T.; Murakami, T. N.; Snaith, H. J. Efficient Hybrid Solar Cells Based on Meso-Superstructured Organometal Halide Perovskites. *Science* **2012**, *338*, 643−647.

(23) Ball, J. M.; Lee, M. M.; Hey, A.; Snaith, H. J. Low-Temperature Processed Meso-Superstructured to Thin-Film Perovskite Solar Cells. *Energy Environ. Sci.* **2013**, *6*, 1739−1743.

(24) Abate, A.; Hollman, D. J.; Teuscher, J.; Pathak, S.; Avolio, R.; D'Errico, G.; Vitiello, G.; Fantacci, S.; Snaith, H. J. Protic Ionic Liquids as P-Dopant for Organic Hole Transporting Materials and Their Application in High Efficiency Hybrid Solar Cells. *J. Am. Chem. Soc.* **2013**, *135*, 13538−13548.

(25) Im, J.-H.; Lee, C.-R.; Lee, J.-W.; Park, S.-W.; Park, N.-G. 6.5 Efficient Perovskite Quantum-Dot-Sensitized Solar Cell. *Nanoscale* **2011**, *3*, 4088−4093.

(26) Liu, M. Z.; Johnston, M. B.; Snaith, H. J. Efficient Planar Heterojunction Perovskite Solar Cells by Vapour Deposition. *Nature* **2013**, *501*, 395−398.

(27) Burschka, J.; Pellet, N.; Moon, S. J.; Humphry-Baker, R.; Gao, P.; Nazeeruddin, M. K.; Grätzel, M. Sequential Deposition as a Route to High-Performance Perovskite-Sensitized Solar Cells. *Nature* **2013**, *499*, 316−319.

(28) Lee, J.-W.; Lee, T.-Y.; Yoo, P. J.; Grätzel, M.; Mhaisalkar, S.; Park, N.-G. Rutile TiO_2-Based Perovskite Solar Cells. *J. Mater. Chem. A* **2014**, *2*, 9251−9259.

(29) Docampo, P.; Hanusch, F. C.; Stranks, S. D.; Döblinger, M.; Feckl, J. M.; Ehrensperger, M.; Minar, N. K.; Johnston, M. B.; Snaith,

DOI: 10.1021/acsami.5b01330
ACS Appl. Mater. Interfaces 2015, 7, 9645−9651

H. J.; Bein, T. Solution Deposition-Conversion for Planar Heterojunction Mixed Halide Perovskite Solar Cells. *Adv. Energy Mater.* **2014**, DOI: 10.1002/aenm.201400355.
(30) Liu, D.; Gangishetty, M. K.; Kelly, T. L. Effect of $CH_3NH_3PbI_3$ Thickness on Device Efficiency in Planar Heterojunction Perovskite Solar Cells. *J. Mater. Chem. A* **2014**, *2*, 19873−19881.
(31) Wu, Y.; Islam, A.; Yang, X.; Qin, C.; Liu, J.; Zhang, K.; Peng, W.; Han, L. Retarding the Crystallization of PbI_2 for Highly Reproducible Planar-Structured Perovskite Solar Cells Via Sequential Deposition. *Energy Environ. Sci.* **2014**, *7*, 2934−2938.
(32) Malinkiewicz, O.; Yella, A.; Lee, Y. H.; Expallargas, G. M.; Grätzel, M.; Nazeeruddin, M. K.; Bolink, H. J. Perovskite Solar Cells Employing Organic Charge-Transport Layers. *Nat. Photonics* **2014**, *8*, 128−132.
(33) Zhou, H.; Chen, Q.; Li, G.; Luo, S.; Song, T.; Duan, H. S.; Hong, Z.; You, J.; Liu, Y.; Yang, Y. Interface Engineering of Highly Efficient Perovskite Solar Cells. *Science* **2014**, *345*, 542−546.
(34) You, J.; Hong, Z.; Yang, Y.; Chen, Q.; Cai, M.; Tze-Bin, S.; Chen, C.; Lu, S.; Liu, Y.; Zhou, H. Low-Temperature Solution-Processed Perovskite Solar Cells with High Efficiency and Flexibility. *ACS Nano* **2014**, *8*, 1674−1680.
(35) Jong, M. P. D.; Ijzendoorn, L. J. V.; De, V. M. A. Stability of the Interface Between Indium-Tin-Oxide and Poly(3,4-Ethylenedioxythiophene)/Poly(Styrenesulfonate) in Polymer Light-Emitting Diodes. *Appl. Phys. Lett.* **2000**, *77*, 2255−2257.
(36) Wong, K. W.; Yip, H. L.; Luo, Y.; Wong, K. Y.; Lau, W. M.; Low, K. H.; Chow, H. F.; Gao, Z. Q.; Yeung, W. L.; Chang, C. C. Blocking Reactions Between Indium-Tin Oxide and Poly(3,4-Ethylene Dioxythiophene): Poly(Styrene Sulphonate) with a Self-Assembly Monolayer. *Appl. Phys. Lett.* **2002**, *80*, 2788−2790.
(37) Shrotriya, V.; Li, G.; Yao, Y.; Chu, C. W.; Yang, Y. Transition Metal Oxides as the Buffer Layer for Polymer Photovoltaic Cells. *Appl. Phys. Lett.* **2006**, *88*, No. 073508.
(38) Xu, M. F.; Cui, L.; Zhu, X. Z.; Gao, C. H.; Shi, X. B.; Jin, Z. M.; Wang, Z. K.; Liao, L. S. Aqueous Solution-Processed MoO_3 as an Effective Interfacial Layer in Polymer/Fullerene Based Organic Solar Cells. *Org. Electron.* **2013**, *14*, 657−664.
(39) Liang, J.; Zu, F. S.; Ding, L.; Xu, M. F.; Shi, X. B.; Wang, Z. K.; Liao, L. S. Aqueous Solution-Processed MoO_3 Thick Films as Hole Injection and Short-Circuit Barrier Layer in Large-Area Organic Light-Emitting Devices. *Appl. Phys. Express* **2014**, *7*, No. 111601.
(40) Hung, L. S.; Tang, C. W.; Mason, M. G. Enhanced Electron Injection in Organic Electroluminescence Devices Using an Al/LiF Electrode. *Appl. Phys. Lett.* **1997**, *70*, 152−154.
(41) Schubert, S.; Hermenau, M.; Meiss, J.; Meskkamp, L. M.; Leo, K. Oxide Sandwiched Metal Thin-Film Electrodes for Long-Term Stable Organic Solar Cells. *Adv. Funct. Mater.* **2012**, *22*, 4993−4999.
(42) Xu, M. F.; Shi, X. B.; Jin, Z. M.; Zu, F. S.; Liu, Y.; Zhang, L.; Wang, Z. K.; Liao, L. S. Aqueous Solution-Processed GeO_2: An Anode Interfacial Layer for High Performance and Air-stable Organic Solar Cells. *ACS Appl. Mater. Interfaces* **2013**, *5*, 10866−10873.
(43) Saliba, M.; Wee, T. K.; Hiroaki, S.; Moore, D. T.; Trent, S.; Zhang, W.; Estroff, L. A.; Ulrich, W.; Snaith, H. J. Influence of Thermal Processing Protocol upon the Crystallization and Photovoltaic Performance of Organic−Inorganic Lead Trihalide Perovskites. *J. Phys. Chem. C* **2014**, *118*, 17171−17177.
(44) Hsu, H.-L.; Chen, C. P.; Chang, J. Y.; Yu, Y. Y.; Shen, Y. K. Two-Step Thermal Annealing Improves the Morphology of Spin-Coated Films for Highly Efficient Perovskite Hybrid Photovoltaics. *Nanoscale* **2014**, *6*, 10281−10288.
(45) Bai, S.; Wu, Z. W.; Wu, X. J.; Jin, Y. Z.; Zhao, N.; Chen, Z. H.; Mei, Q. Q.; Wang, X.; Ye, Z. Z.; Song, T. High-Performance Planar Heterojunction Perovskite Solar Cells: Preserving Long Charge Carrier Diffusion Lengths and Interfacial Engineering. *Nano Res.* **2014**, *12*, 1749−1758.
(46) Ali, U. A.; Oyama, M. Growth of High-Density Gold Nanoparticles on an Indium tin Oxide Surface Prepared Using a "Touch" Seed-Mediated Growth Technique. *Cryst. Growth Des.* **2005**, *5*, 599−607.
(47) Vayssieres, L. Growth of Arrayed Nanorods and Nanowires of ZnO from Aqueous Solutions. *Adv. Mater.* **2003**, *15*, 464−466.
(48) Greene, L. E.; Law, M.; Goldberger, J.; Kim, F.; Johnson, J. C.; Zhang, Y. F.; Saykally, R. J.; Yang, P. D. Low-Temperature Wafer-Scale Production of ZnO Nanowire Arrays. *Angew. Chem., Int. Ed.* **2003**, *42*, 3031−3034.
(49) Zuo, F.; Williams, S. T.; Liang, P. W.; Chueh, C. C.; Liao, C. Y.; Jen, A. K.-Y. Binary-Metal Perovskites toward High-Performance Planar-Heterojunction Hybrid Solar Cells. *Adv. Mater.* **2014**, *26*, 6454−6460.

DOI: 10.1021/acsami.5b01330
ACS Appl. Mater. Interfaces 2015, 7, 9645−9651